Study of a Model α-Helix Peptide's Surface Properties by Langmuir Monolayer Techniques and Surface FTIR

by

J. Dale Combs

A Thesis Submitted in Partial Fulfillment

of the Requirements for the Degree of

Master of Science in Chemistry

Middle Tennessee State University

August 2016

Thesis Committee:

Dr. Chengshan Wang, Thesis Advisor

Dr. Ngee-Sing Chong

Dr. Kevin Bicker

ACKNOWLEDGEMENTS

I would like to sincerely thank Dr. Chengshan Wang for his constant support and guidance in my thesis research. I would like to thank Dr. Ngee S. Chong for assisting this research as a committee member and for his guidance as a professor. I would like to thank Dr. Kevin Bicker also for his assistance as a committee member and also for the extensive use of his instruments and slightly less extensive use of his reagents and materials. I would also like to thank Dr. Norma Dunlap and her research group for the use of instruments and for valuable advice. I thank Dr. Leblanc and Dr. Shanghao Li at the University of Miami for the use of their instruments and collaboration.

I would like to thank the MTSU College of Basic and Applied Sciences and College of Graduate studies for hosting and sponsoring events for students like myself to develop and share our research. The MTSU chemistry department has been instrumental in aiding my career development by sponsoring and assisting graduate students in chemistry research and professional development. This has been pivotal for me in achieving goals in graduate school and beyond.

I thank everyone in the chemistry department left unmentioned for your assistance in some way or another, especially Jesse Weatherly. I thank my friends and family, who continue to support me. I am particularly grateful to have a friend and mentor, Dr. Chengshan Wang, who has taken meticulous effort to ensure that my career as a chemist is an exciting one.

ABSTRACT

Cell membranes have been shown to be able to change the conformation of proteins/peptides. However, the structure of the cell membrane is complicated and has been divided to three regions: the hydrophobic region containing alkyl chains, the hydrophilic head group, and the hydration layer, or lipid-water interface, which exists between the hydrophilic head group and the bulk water solution, but with lower dielectric constant compared with fully hydrated water. The air-water interface has been used to mimic the structure of the hydration layer because of their similar dielectric constant.[1,2] Some proteins were found to form a stable Langmuir monolayer and accumulate at the air-water interface. For example, α-synclein, a membrane protein containing 140 amino acids, is unstructured in aqueous solution but changes its conformation to α-helix at the air-water interface. This incites interest to investigate short motifs of α-helix to form a stable Langmuir monolayer at the air-water interface. In this thesis, a peptide with sequence of $YAAAA(KAAAA)_4$ (referred as Pep25 hereafter) was used as a model peptide of α-helix to spread at the air-water interface, because our group has determined the conformation of Pep25 in residue level by the ^{13}C isotope-edited FTIR. Langmuir monolayer technique together with IRRAS showed that Pep25 does not form a typical Langmuir monolayer at the interface. Potential plans to make Pep25 to form a stable monolayer are also discussed in this thesis.

TABLE OF CONTENTS

LIST OF FIGURES

LIST OF TABLES

CHAPTER 1 INTRODUCTION

1.1 Structural Biology

Polypeptides are complex macromolecules, which are biosynthetic polymers composed of monomers called amino acids.[3] Large polypeptides with more than 200 residues are termed proteins, smaller ones are termed peptides.[3] Biosynthetic polypeptides are commonly composed of 20 different amino acids shown in Table 1. As shown in Figure 1, amino acids consist of one amino group, one carboxylic acid group, and an sp^3 hybridized α-carbons bound to a residue group, the R group. The polymeric backbone is a sequence of sp^3 hybridized α-carbons covalently linked to amide bonds.[3-6] The residue group determines the identity of the amino acid. The combination and sequential arrangement of R groups in the polypeptide determines its chemical and physiological properties.

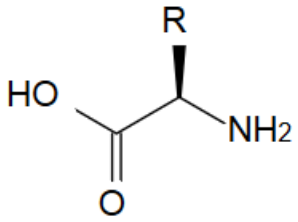

Figure 1. Amino acid chemical structure

Table 1. Amino acid R group chemical structure, name, three letter, and one letter abbreviation.

Lysine **Lys K** 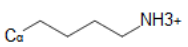	**Asparagine** **Asp N** 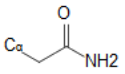	**Leucine** **Leu L** 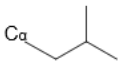
Histidine **His H** 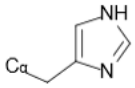	**Glutamine** **Gln Q** 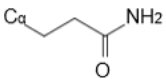	**Methionine** **Met M** 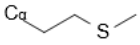
		Tyrosine **Tyr Y** 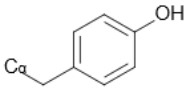
Arginine **Arg R** 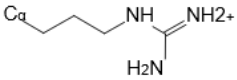	**Glycine** **Gly G** 	
		Cystein **Cys C** 
Aspartic Acid **Asp D** 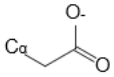	**Proline** **Pro P** 	**Tyrptophan** **Trp W** 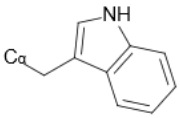
	Alanine **Ala A**	
Glutamic Acid **Glu E** 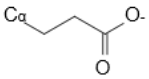	**Valine** **Val V** 	**Phenylalanine** **Phe F** 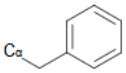
		Threonine **Thr T** 
Serine **Ser S** 	**Isoleucine** **Ile I** 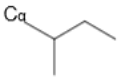	

Peptides and proteins are essential in biochemical processes, especially as enzyme catalysts in metabolic reactions,[7-11] DNA replication,[12,13] and biochemical signal transduction.[14,15] Malfunction of proteins through structural distortion is implicated in many human diseases.[7,9,10,16-19] The elucidation of protein structure has aided both the understanding of their biochemical mechanisms and provided information relevant to their pathology. Structural biology, which emphasizes the elucidation of protein structure is a growing scientific discipline.[20-23] For example, the

determination of the structure of a protein critical to photosynthesis was awarded the Nobel Prize in 1988[20] and the 2009 Nobel Prize was awarded to Venkatraman Ramakrishnan, Thomas A. Steitz, and Ada Yonath for the elucidation of the structure of ribosome, an important biomolecule partially composed of polypeptide.[10,21,22]

1.2 Polypeptide Structure

1.2.1 Primary Structure

Amino acids are covalently linked together by an amide bond (i.e., CO-NH), formed between the amine group of one amino acid and the carboxyl group of the adjacent amino acid.[5] A chain of amino acids connected by amide bonds is referred to as a polypeptide chain. A polypeptide's primary structure refers to the sequential arrangement of amino acids in the polypeptide chain. The two termini of a polypeptide chain are called N-terminus (containing a free amine group) and C-terminus (containing a free carboxylic acid group). The primary structure of a polypeptide is usually written from N-terminus to C-terminus. Figure 2 is an example of protein primary structure of Pep25 with 25 residues, which is the focus of this thesis. One letter abbreviations are used to designate one polymerized amino acid and its characteristic residue group. These abbreviations are particularly useful in denoting the sequence of long proteins, which may be thousands of residues in length.

YAAAAKAAAAKAAAAKAAAAKAAAA

Figure 2. Primary structure of Pep25, a model α-helical peptide. (*cf.* Table 1)

1.2.2 Secondary structure

Secondary structure is the local conformation of the amide backbone. It is characterized by the intra and intermolecular hydrogen bonds among the amino acid residues.[22] Different segments, or stretches primary structure, on a single polypeptide molecule may have different secondary structures. Typical secondary structures (also called conformations) include α-helix, β-sheet, and random coil, which also called unstructured conformation.[2,24,25] A conformation of random coil denotes the lack of a regular secondary structure, the polypeptide chain in this structure is well dissolved in the aqueous solution, and moves freely in the aqueous environment.[2] In random coil the residues in the polypeptide chain do not substantially form hydrogen bonds with each other, but form hydrogen bonds with solvent H_2O molecules in solution.[22]

As the most common secondary structure, the α-helix looks like a spring as shown in Figure 3 a. It is characterized by the intra-molecular hydrogen bonds between the amino group of one amino acid and the carbonyl group of another amino acid located 4 residues away along the polypeptide chain (*cf.* Figure 3 a).[25] The orientation of the hydrogen bonds between the amide carbonyl of one group and the amide nitrogen of the coupled group are usually parallel to the helical axis.[25] The biosynthetic α-helix is typically right handed and has a pitch of approximately 3.6 amino acid residues per turn.[25] The formation of hydrogen bonds create a helical structure of the polypeptide

chain. Residue groups of polypeptides in α-helix conformation protrude outwards from the helical axis.[25]

The structural units of β-sheets are rigid linear strands, which are characterized by multiple strands (polypeptide chains) arranged side-by-side as shown in Figure 3 b.[24] Each β-sheet contains 6 to 22 strands. Residue groups are present above and below the plane of hydrogen bonding backbones. Inter-strand hydrogen bonds are formed between the carbonyl oxygen of one chain and the amide hydrogen of another chain.[24]

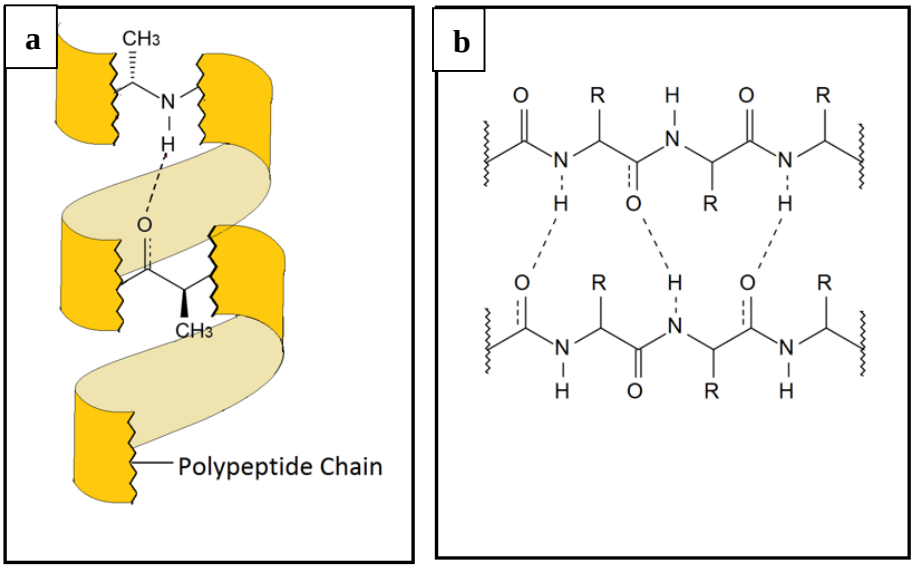

Figure 3. Illustration of α-helix (a, left), and β-sheet (b, right) secondary structures.

1.2.3 Tertiary structure

Secondary structure elements compose to form a well-defined 3D structure called tertiary structure.[26,27] Polypeptide tertiary structures arise predominantly from four forces: hydrophobic forces, covalent bonds, van der Waals interactions, and hydrogen bonds. Hydrophobic interactions arising from secondary structural elements are crucial in stabilizing tertiary structure, also referred to as the native state of the

protein.[27] It is common for residues that are far away in the primary structure to be spatially in close proximity to each other in the tertiary structure. In biological systems, other factors, such as the cell membrane, can affect the structures of polypeptides as discussed below.

1.3 Amphiphilic Structures and Phospholipid Bilayers in Biological Systems

Phospholipids are composed of a hydrophobic group, usually of alkyl chains, and a hydrophilic head group, usually joined together by a glycerol molecule which is linked to a phosphate group. The phosphate group can be covalently linked to various head groups, such as choline, ethanolamine, serine, and others. A common phospholipid in cells is dipalmitoylphosphatidylcholine (DPPC), the structure of DPPC is shown in Figure 4.[28] Due to their amphiphilic nature, phospholipids can form a bilayer structure. In an amphiphilic bilayer structure, the hydrophobic alkyl chains orient to contact each other and form an inner hydrophobic layer. The hydrophilic head groups of one phospholipid layer contacts the external aqueous environment and the head groups of the other layer contact the internal aqueous environment to form two surfaces as shown in Figure 5.[28] The most common types of bilayer structures are liposomes and cell membranes.

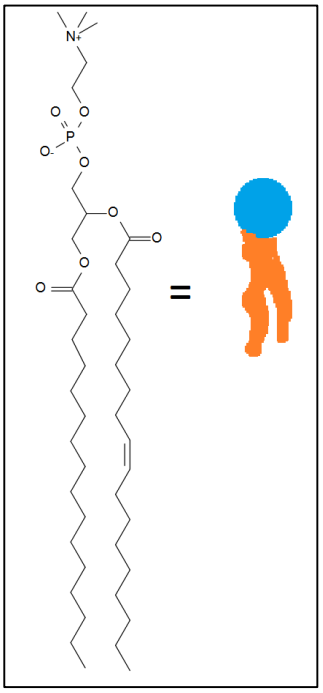

Figure 4. Dipalmitoylphosphatidylcholine chemical structure.

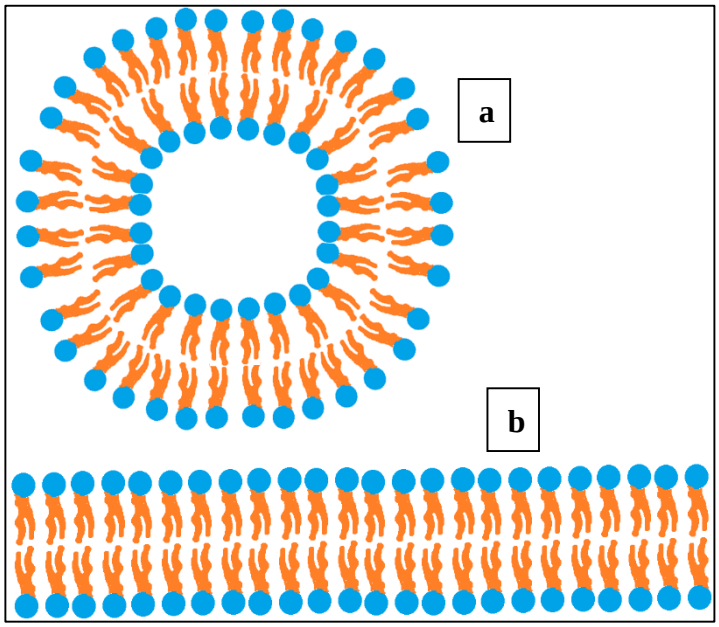

Figure 5. Liposome (a, top), planar phospholipid bilayer (b, bottom).

Liposomes are spherical phospholipids bilayer structures with a curved surface, as shown in Figure 5a.[29] One of the two hydrophilic surfaces faces the exterior aqueous environment and the other surface faces the interior core of the liposome. Hydrophilic solutes in the bulk aqueous solution cannot penetrate the hydrophobic layer to reach the aqueous core inside the liposomes. Similarly, the solutes in the membrane bound aqueous core cannot escape the liposome and diffuse to the bulk aqueous solution, either. Thus, liposomes exist widely in cells to encapsulate various chemicals such as neurotransmitters, and can fuse into and become part of the cell membrane.[30] The structure of the cell membrane is discussed below.

Cell membranes, although being another phospholipid bilayer structure, have less surface curvature compared with liposomes, (as shown in Figure 5 b), due to their much larger size. Different cells, all of which have a phospholipid bilayer cell

membrane, may have a diverse array of shapes.[31] In contrast, liposomes all have a roughly spherical shape. Thus, extended planar phospholipid bilayer structures have been used to mimic the cell membrane.[32] If cells are "houses", cell membrane is the "wall" of the "house" and have the same permeation properties as liposomes with regards to solutes as discussed previously. Polypeptides embed in cell membranes or liposomes and play a wide array of biochemical roles. They function as hormones, cell signaling agents, and affect the rheological properties of the membrane.[33] Maintenance of cellular homeostasis is often accomplished by membrane bound channel forming proteins.[34] Therefore, the interaction of polypeptides with phospholipid bilayers are important subjects of scientific research.

1.4 Model System of Amphiphilic Structures in Biological Systems

The structure of phospholipid bilayers is variable and complex. The structure may be divided into separate regions with distinct chemical characteristics. The interior of the bilayer is composed of the hydrophobic alkyl chains of the two layers of phospholipids. This is termed the hydrophobic region. The second region towards the solution is made up of the compacted hydrophilic head groups of the phospholipids.[35] These head groups may have a charge which varies with the previously discussed chemical structure of the head group.[36] The barrier between the bulk aqueous environment and the phospholipid head groups is the third and last region. This is the lipid-water interfacial layer which is about 4 to 5 water molecules thick.[36] This layer is composed of water molecules which have an electrostatic structure influenced by the

phospholipid head groups which they contact.[35] These water molecules have a structure which is different than that of the bulk solution. Evidence for this is that the dielectric constant of this layer is different than that of the bulk solution.[1] Such a complexicity makes it difficult to study the interaction between molecules at the phospholipid bi-layer and model systems have been developed.

1.5 Langmuir Monolayers at the Air-Water Interface

It has been shown that the physical characteristics, such as the dielectric constant, of the air-water interface are similar to the third region of the phospholipid bilayer, i.e. the lipid-water interface, thus, the air-water interface has been used as a model system. It has been shown that various amphiphilic molecules arrange in layers of single molecules at the air-water interface, such a layer is referred to as a Langmuir monolayer (LM).[2] Most molecules of sufficient size and amphipathic chemistry form LM's at the air-water interface. Compared with phospholipid bilayer structures, the physical parameters, such as distance between molecules, of the air-water interface can be more easily monitored by various techniques as shown below.

One such technique is measuring the surface pressure of the air-water interface while reducing the surface area. This is accomplished using an instrument called a Langmuir trough, which is diagramed in Figure 6. A Langmuir trough consists of a rectangular trough which contains the solution, called the subphase, with the edges of the exposed surface surrounded by hydrophobic barriers which are usually made of polytetrafluoroethylene. Molecules which may form a LM are deposited on the surface

with a syringe. The two shorter sides of the rectangular surface may be mechanically compressed, allowing the subphase to pass underneath. Any LM forming molecules will be trapped between the barriers. Because both the available surface area and amount of substance deposited on the surface is known, they can be used to measure the molecular area; the distance between the molecules at the surface. As the molecular area decreases the molecules will be compressed together. This compression will result in molecular interactions, which increase the surface pressure of the interface to which the molecules are confined. This increase in surface pressure is detected by an inert probe which contacts, but does not significantly penetrate, the surface of the air-water interface via the decreasing tension it exerts on a mass balance from which it hangs.

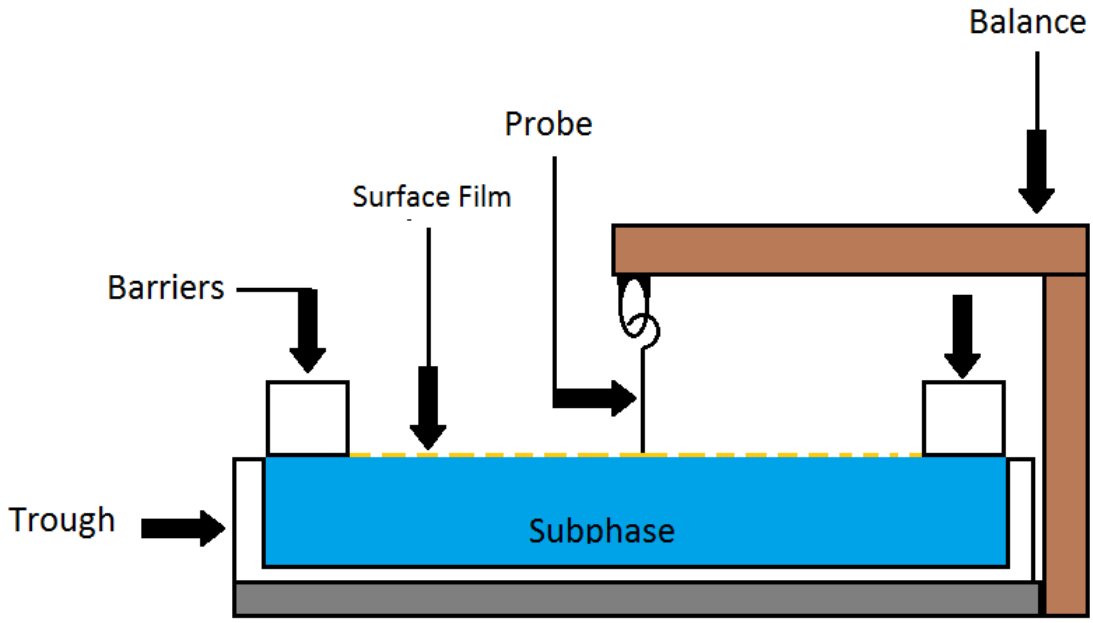

Figure 6. Langmuir trough diagram.

Typically, a decreasing slope will be detected in the graph of surface area versus surface pressure, which is called a compression isotherm, or surface pressure/area (π-A) isotherm. The shape of the π-A isotherm of a molecule indicates whether or not the

molecule forms a LM on the surface. One such molecule widely used to study LM's is stearic acid [37]. The structure of stearic acid is shown in Figure 7.

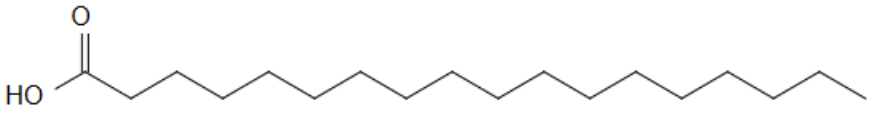

Figure 7. Chemical structure of stearic acid.

Aside from small amphiphilic molecules, polypeptides can also form a LM. A π-A of a LM of one such peptide, α-synuclein is shown in Figure 8.[38] This peptide has has several α-helical segments at the air-water interface and cell-membrane, and is implicated in the pathology of Parkinson's Disease [2]. The peptide is unstructured in aqueous solution, but changes its conformation to α-helix at the air-water interface to form a stable LM.[2] As shown below, the slope of the π-A isotherm of α-synucein is steep, indicating the presence of a LM.[2]

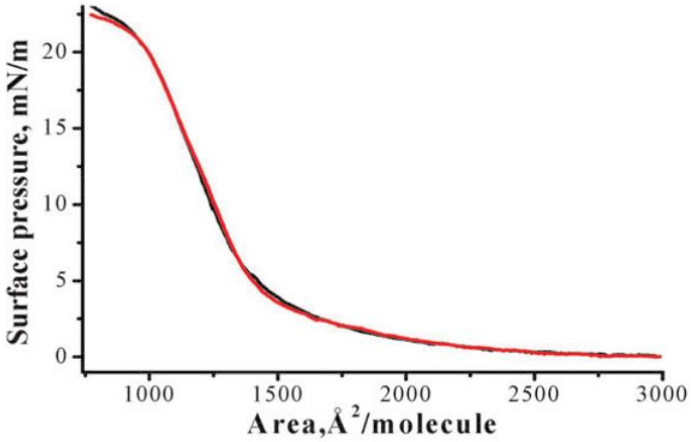

Figure 8. π-A of α-Synuclein, Adapted With Permission From Reference 2.

The advantages of the Langmuir trough technique as a model of a phospholipid bilayer as opposed to studying the structure directly is that the surface pressure can be detected and controlled. Different molecular packing environments can be studied by

compressing the surface to a specific pressure and making analytical measurements, modifying the bulk subphase, or depositing molecules onto the surface.[2,39] A major advantage of the Langmuir trough technique is the ability to collect FTIR spectroscopic information selectively for molecules at the surface, excluding molecules in the bulk water subphase from the spectra. This provides the unique opportunity to study both the secondary structure and orientation of polypeptides in physiological states by measuring the wavelengths of infrared radiation absorbed. These techniques and strategies are discussed in the next section.

1.6 FTIR Spectroscopy

The absorption of infrared (IR) radiation is a widely used spectroscopic technique to probe the secondary structure of peptides. [2,40-49] The advantage of IR spectroscopy over other techniques is that it can be applied to a range of sample states like gasses, crystalline solids, amorphous solids, and solutions. IR spectroscopy requires a small amount, or a low concentration, for effective measurement. Membrane proteins can be analyzed by this method.[2,43-45,48,49] Fourier Transform Infra-Red (FTIR) spectrometers make it possible to acquire spectra of high accuracy with facile methodology.

In FTIR spectroscopy, the amide functional group of the backbone of the polypeptide backbone absorbs infrared radiation, giving rise to nine characteristic 'Amide' IR bands namely Amide A, B, and I through VII.[2,43-45,48] Frequency ranges and descriptions of these amide bands are shown in Table 2. Particularly, the Amide I and Amide II bands are the most prominent bands in polypeptide spectra.[41] The Amide I

band absorption ranges from 1600-1700 cm^{-1}, the C=O stretching vibrations of the amide carbonyl contributes around 85% to this band.[50] For the Amide II band, the amide N-H bending vibration contributes 40-60%, along with C-N stretching vibrations, which contribute around 18-40%, but is less responsive to the secondary structural changes of polypeptides than the Amide I band.[51] All other bands are composed of overlapping frequencies of the vibrations of multiple functional groups and are not yet widely used for secondary structural studies.

Table 2. Characteristics infrared bands of polypeptide amide bonds.

Designation	Approximate Frequency (cm^{-1})	Description
Amide A	3300	NH stretching
Amide B	3100	NH stretching
Amide I	1600-1690	C-O stretching
Amide II	1480-1575	CN stretching, NH bending
Amide III	1229-1301	CN stretching, NH bending
Amide IV	625-767	OCN bending
Amide V	640-800	Out-of-plane, NH bending
Amide VI	537-606	Out-of-plane, C-O bending
Amide VII	200	Skeletal torsion

In the Amide I region (1600-1700cm^{-1}), each type of secondary structure gives rise to a unique peak absorption frequency range arising from characteristic differences in hydrogen bonding patterns.[43,45,48] Some of these peak absorption frequency ranges characteristic of different types of secondary structures are shown in Table 3. For example, unstructured conformation shows a peak at ~1640 cm^{-1} for the Amide I band and the peak of β-sheet is ~1630 cm^{-1}. For α-helical segments, the peak position is

significantly affected by the length of the helix. For a long helix, the peak will appear at ~1648 cm^{-1} and shifts to higher frequency as the helix becomes shorter.[50,52,53]

Table 3. Characteristic amide I frequencies of protein secondary structures.

Frequency(cm^{-1})	Assignment
1690-1680	β-sheet structure
1657-1648	helix
1645-1640	Random coil
1630-1620	β-sheet structure

The aspect of FTIR important to the study of polypeptides at the air-water interface, and especially peptides in short-lived transient states, is that spectra can be obtained quickly; from several seconds to minutes, depending on the number of scans taken. FTIR spectroscopy has evolved into a powerful probe of conformational analysis of proteins/peptides in solution, as well as the orientation of peptides at the air-water interface.[2] FTIR can be used to detect the presence and characterize the secondary structure of molecules at the interface by infrared reflection-absorption spectroscopy (IRRAS), as detailed below.

1.7 IRRAS

IRRAS involves reflecting the incident IR light beam from a surface. To study the conformation of peptides at the air-water interface, that surface is the air-water interface. To study molecules at the interface, the orientation of the polarity of the electric and magnetic field vectors of the incident radiation is controlled. This is called polarizing the electromagnetic radiation.

Orienting the electric field vector, also called the p-vector, of the incident IR beam parallel to the normal of the air-water interfacial plane is called p-polarized IRRAS. A diagram of p-polarized IRRAS is given in Figure 9. This type of IR spectroscopy will result in a characteristic absorption spectrum that changes with the orientation of the molecules at the interface.[2] Molecules at the surface which have a random orientation relative to the air-water interface plane will not have significant peaks in the p-polarized IRRAS spectrum.[2] Water molecules, buffer salts, and randomly oriented surface species are not favored by the selection rules of p-polarized IRRAS.[2] This creates the advantage of eliminating IR spectral bands which may overlap those bands of interest, such as the O-H band of water overlaps the Amide I band of polypeptides.

To determine the interfacial orientation of IR active groups, the angle of incidence of the IR beam must be varied according to the methodology used by Wang et. al.[2] Several p-polarized IRRAS spectra are taken at angles above and below the Brewster angle. The Brewster angle is the angle of incidence at which no polarized light is reflected from the surface. This angle varies with the varying chemical makeup of the surface, for water it is 54.2° from the surface normal.[40]

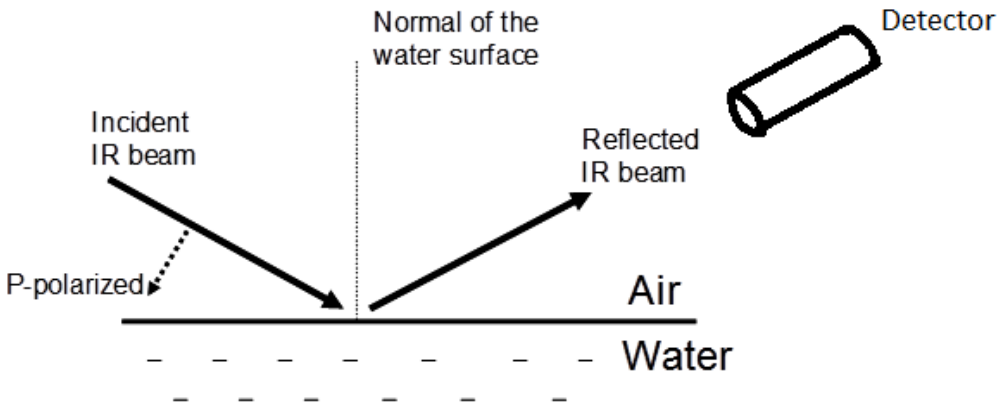

Figure 9. Diagram of p-polarized IRRAS.

Functional groups with a defined orientation relative to the plane of the air-water interface, either parallel or perpendicular, will display peaks in the p-polarized IRRAS spectrum. These peaks are the IR absorbance of the oriented functional groups which show the same secondary structure dependent peak shifting behavior as discussed for traditional FTIR spectroscopy (c.f. Table 3). Therefore, the secondary structure of peptide chains which have a defined orientation at the interface can be probed as discussed previously.[2]

The orientation of peptide chains, weather parallel or perpendicular to the surface, can also be determined by p-polarized IRRAS.[2] An example of this methodology is the surface orientation of the LM forming peptide α-synuclein. When an IR absorbing functional group is parallel to the reflecting surface, its IR peaks displays the following pattern in the variable angle p-polarized IRRAS spectra. At incident angles below the Brewster angle, the IRRAS peak will be negative, and its negative intensity will increase as the incident angle increases, as can be observed for Amide I band in the 30°, 35°, and 40° spectra for α-synulein in Figure 10 below. Spectra taken at incident angles

above the Brewster angles will show positive peaks, and the positive intensity of the peaks will decrease as the incident angle increases. The Amide I band shows this pattern for the spectra taken at 60°, 65°, and 70° in Figure 10 below which is the p-Polarized IRRAS of a LM of α-synulein.[2]

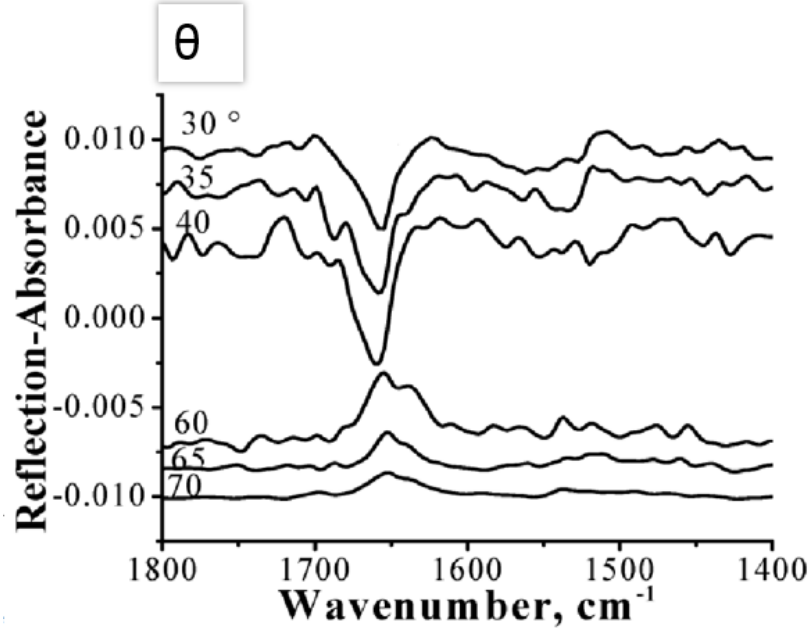

Figure 10. P-Polarized IRRAS spectra of α-synuclein Langmuir monolayer at various incident angles at a surface pressure of 10 mN/m, adapted with permission from reference 2.[2]

Studies have shown that α-helix conformation stabilizes polypeptides at the air-water interface. For example, α-synuclein has an unstructured conformation in bulk aqueous solution and transforms to α-helix conformation at the air water interface.[2] This also supports the model of the air-water interface as the cell membrane hydration layer, as many membrane bound proteins have α-helical segments which stabilize them in the cell membrane.[34] This study addresses the orientation and stability of small model α-helix peptides at the air water interface. While α-synuclein is unstructured in solution

but α-helix at the air water interface. Some small LM forming peptides are α-helix both in solution and during penetration of the cell membrane, while others show the same behavior as α-synuclein and only transform in α-helix upon interaction with bi-layers.[54,55]

1.8 Thesis Proposal

Do α-helical segments prefer a parallel, perpendicular, or random orientation at the air-water interface? The repeating sequence $YAAAA(AAAAK)_n$ has been shown to be a model α-helix in solution. However, when the sequence is of length n = 3, the peptide is in unstructured conformation in pH < 12 solutions. [56] When the sequence is of length n = 4, the peptide is in α-helix conformation in neutral and physiological pH solutions.[57] The length of α-synuclein, which is 140 residues, may play a role in the orientation of its α-helical segments at the air-water interface. Because α-synuclein still has unstructured residues at the air-water interface, they may influence the orientation of its α-helical residues.

To address this, the model alpha helix peptide Pep25, which is composed of the repeating sequence mentioned above with n = 4 will be investigated as to whether it forms a LM at the air-water interface. Every residue of the peptide has been confirmed to be in α-helical conformation, therefore, the peptide should have a roughly linear structure.[57] This will result in all of its carbonyls being oriented parallel to each other, and parallel to the length of the peptide. If it forms a LM, then orientation and conformation will then be investigated at the air-water interface. This will provide

insight into the physio-chemical properties of α-helical peptides and α-helical segments of proteins.

CHAPTER 2. MATERIALS AND METHODS

2.1 Solid Phase Peptide Synthesis

To produce pure Pep25, solid phase peptide synthesis utilizing the Fmoc protection strategy was utilized. Flourenylmethoxycarbamate (Fmoc) is used as a protecting group for the amino group of amino acids to prevent solution coupling of dissolved amino acids. Free amino acid side chains are protected with base-stable protecting groups as follows: t-butyl for phenol on the tyrosine side chain, and tert-butoxycarbanyl protected amino side chains on lysine. The solid support used was Wang resin; 100-200 mesh beads of polystyrene polymer functionalized at a density of 0.7 mM/g with p-hydroxybenzyl alcohol groups to which the amino acid carboxyl attaches. The target peptide is synthesized from C-terminus to N-terminus on a scale of 0.35 mM. Two molar equivalents of protected amino acid and coupling agents were reacted for each coupling step. The reaction volume for all Steps is 10 mL.

The first step in Fmoc-peptide synthesis is coupling the C-terminal residue to the resin, which is accomplished by activating the carboxyl group on the free amino acid with diisopropylcarbodiimide (DIC), using hydroxybenzoyltriazole (HOBt) to suppress racemization. For the first amino acid coupling, which couples the C-terminal amino acid to the resin, 0.1 molar equivalents to Wang resin of 4-dimethylaminopyridine (DMAP) was used to catalytically accelerate activation of the amino acid carboxyl. The solvent for the coupling step is dimethylformamide (DMF) in which the reactants are agitated for three hours. When the reaction is complete the reactants are removed by washing with DMF and diethyl ether, retaining the solid resin through the vessels glass

frit. Deprotecting the resin bound residue is accomplished by suspending and agitating the resin in a 1:4 Piperidine/DMF (v/v) solution for 15 minutes to react with the base labile Fmoc group. Removing the Fmoc protecting group prepares the resin bound amino acid to be coupled to the next residue in the sequence, which is accomplished by the procedure as described above with the coupling time decreased to 30 minutes for the remaining 24 residues.

Coupling and deprotection steps are repeated using the Fmoc protected amino acid indicated in the primary structure of the target peptide. When the peptide chain is complete, the peptide is removed from the resin by washing with dichloromethane (DCM), then suspending the resin in 20 mL trifluoroacetic acid (TFA)/DCM/triisopropylsilane/H_2O 75:22:1.5:1.5 (v/v/v/v), then agitating the suspension to break the bond between the peptides C-terminal carboxyl and resin, and dissolve the peptide into the acid. Triisopropylsilane and H_2O are used to scavenge the t-butyl and tert-butoxycarbanyl protecting groups cleaved by the acid. These synthesis steps are illustrated in Figures 11-13. DCM is used to wash the synthesis vessel after cleaving the peptide, and the wash is combined with the TFA solution. TFA and DCM are then removed via purging with nitrogen gas, then the peptide is precipitated in ethyl ether. The peptide is then pelleted from the ether using mild centrifugation in a 15 mL polypropylene tube. The resulting pellet was dried under vacuum to obtain the crude synthetic peptide.

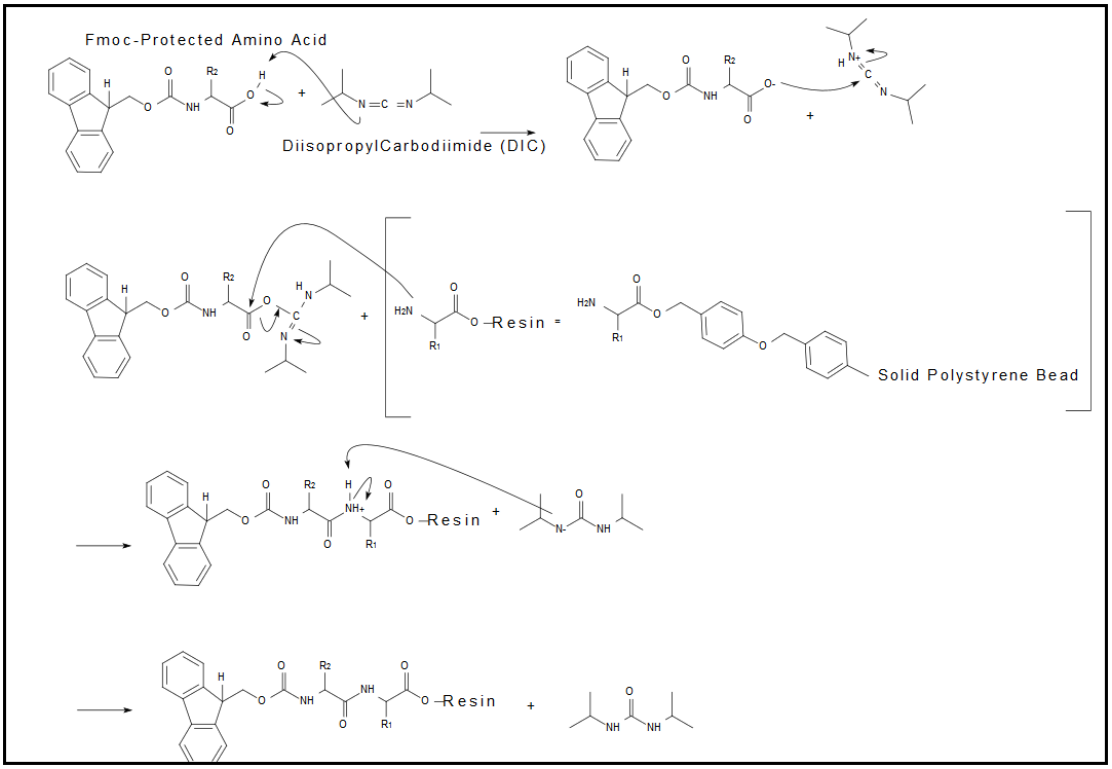

Figure 11. Peptide synthesis coupling reaction

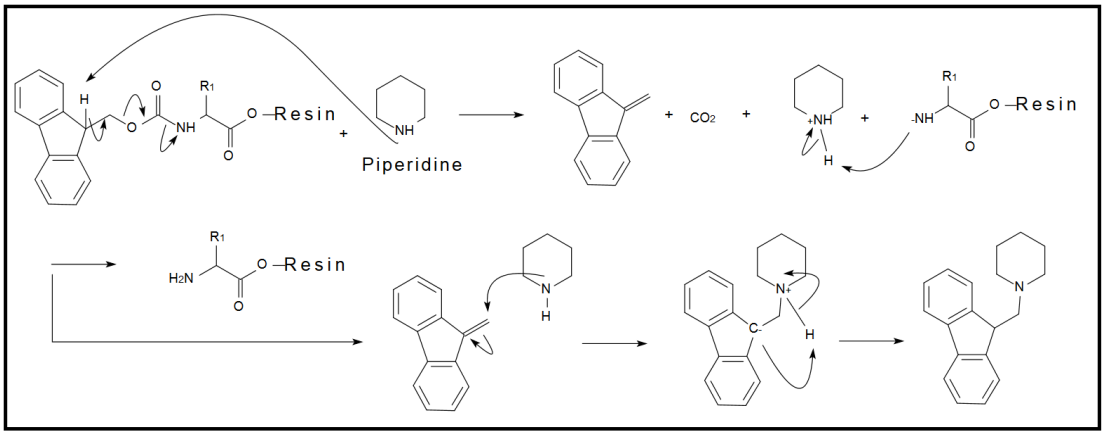

Figure 12. Peptide synthesis deprotection reaction

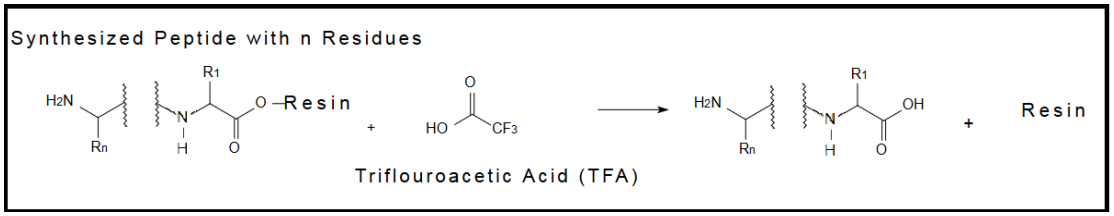

Figure 13. Peptide synthesis cleavage reaction

2.2 Mass Spectrometry

Mass Spectrometry (MS) provides a measure of the molecular weight (MW) distribution of the compounds in a sample. This is accomplished by three basic steps. The first step is to ionize the sample molecules. This is accomplished by a variety of methods, the method used in this research is electrospray ionization. This involves expelling the liquid sample from a small capillary to create an aerosol which is ionized by a coulombic charge on the capillary. The next step is to accelerate the ionized compounds towards the detector via an electric field gradient. For the third step, while the ions move towards the detector, a mass analyzer separates them based on their mass to charge ratio. The mass analyzer used in this research is a Time of Flight (ToF) mass analyzer, which utilized a magnetic field to separate the moving ions. This enables the analysis of the MW of the ions. Pep25 crude product was dissolved in pure water and injected into the MS. The MS chromatogram was collected at a capillary ionization voltage of 3.00 keV.

2.3 MS/MS Fragmentation Analysis

MS/MS fragmentation analysis separates defined mass to charge (M/Z) ratio compounds in one mass analyzer, which separates compounds based on their M/Z ratio. The first mass analyzer in this instance is a quadrupole. The selected molecule then undergoes gas phase collision with a high energy inert gas to break apart the molecule into smaller molecular fragments. The fragments are then separated by another mass analyzer, a ToF mass analyzer in this research, to identify their MW. The MW of the

fragments may then be analyzed to interpret the structure of the selected M/Z ratio molecule. A diagram of the technique is shown in Figure 14.

In polypeptides, the most probable fragmentation site is the bond between the amide carbonyl carbon and amide nitrogen, as illustrated in Figure 14. To analyze Pep25 a table of possible fragments and their theoretical MW was generated to compare to the M/Z peaks in the fragmentation mass spectrum.

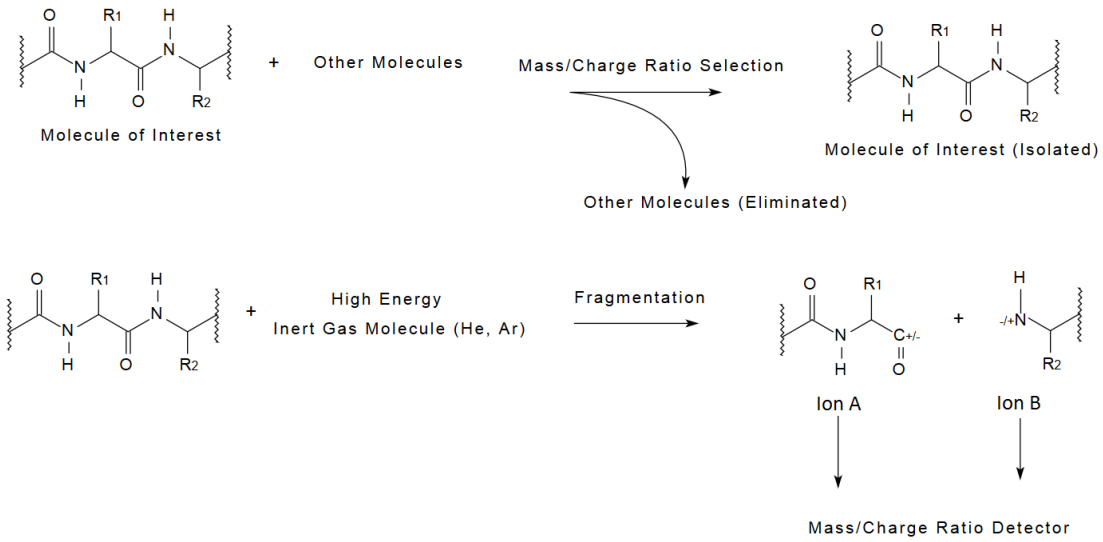

Figure 14. MS/MS fragmentation diagram and breaking of amide bond.

Both MS and MS/MS Fragmentation Analysis was carried out on a Waters Synapt G2 Electrospray Ionization (ESI)-TOF mass spectrometer (Waters Corp., Milford, MA). Spectra were collected from HPLC purified Pep25 dissolved in pure water. Ionization of the molecule was accomplished at a capillary voltage of 3.00 keV. The peak selected for fragmentation was the doubly charged ion of Pep25 with a M/Z ratio of 1058.3 Da/q. The collision energy was set to 35 keV, the inert gas used was argon. The resulting fragmentation mass spectrum was collected between 0 and 2500 M/Z to observe fragments of Pep25.

2.4 High Performance Liquid Chromatography

High performance liquid chromatography (HPLC) separates compounds based on their affinity to the functionality of the surface of porous material packed into a chromatographic column. Their affinity is manipulated by controlling the identity and concentration of solvents used to dissolve the analyte. When the column packing material surface is functionalized with a hydrophilic functionality, the technique is termed normal phase HPLC. When the material is functionalized with a hydrophobic functionality, the technique is termed reverse phase HPLC.

HPLC was carried out on a Waters 1525 Binary Solvent Pump (Waters Corp., Milford, MA) attached to a Phenomenex Reverse Phase Semi Prep C18 Column (Model Jupiter-00G-4055- P0) with column dimensions of 21.5 mm internal diameter and 250 mm length) (Phenomenex, Inc. Torrence, CA). Detection was accomplished via monitoring UV absorbance at 220 nm and measured by a waters 2489 UV-Vis detector (Waters Corp., Milford, MA). Separation of Pep25 from impurities in the crude product was accomplished by a linear gradient of 8-16% A:B (v/v) at a flow rate of 21.2 mL/minute for 40 minutes using water/0.1% TFA (v/v) as mobile phase A, and acetonitrile/0.1% TFA (v/v) as mobile phase B. The retention time of Pep25 was identified by fractionation and MS. After confirmation of the MW of Pep25 in the fraction, chromatography was repeated, the collected fractions were then frozen at -80 ° C and lyophilized to obtain the solid purified Pep25.

2.5 UV Spectrophotometry Concentration Quantitation

Due to hydration layers on the solid purified peptide which contribute to the mass of the solid as measured by an analytical balance, UV-spectrophotometry was used to accurately determine the concentration of Pep25 in the solution spread at the air-water interface. UV-spectrophotometry was carried out on a Hitachi U2900 UV-Vis spectrophotometer (Hitachi High-Technologies Corporation, Tokyo, Japan). Samples were dissolved in pure water and measured in a quartz cuvette with a 1 cm path length, pure water was used as the background. Absorbance was measured in a wavelength range from 250 to 300 nm at a scan speed of 100 nm/minute to quantify the absorption from the single aromatic tyrosine residue of Pep25. Standard solutions of free tyrosine amino acid of concentrations 0.1, 0.2, 0.4, 0.6, 0.8, and 1.0 mM were measured to construct a linear plot of concentration v.s. absorbance and derive the molar absorptivity of the phenol residue group. The concentration of the Pep25 solution used for surface area-pressure isotherms was derived by diluting the solution at a 1:4 ratio with pure water, measuring the absorbance at 275 nm and plotting the absorbance on the aforementioned linear calibration curve.

2.6 Langmuir Trough π-A Isotherm

A Kibron µtrough X Langmuir trough (Kibron Inc., Helsinki Finland) was used for the acquisition of π-A isotherms of Pep25. Pep25 was measured on subphases pure water, 0.1 M phosphate buffered saline pH 7.2, carbonate buffer pH 10.1, and phosphate buffered saline pH 11.9. All subphases used were made up with 18.2 MΩ H_2O. π-A

isotherms of pure subphase were measured and taken as zero surface pressure prior to spreading Pep25 solution on the surface (results not shown). The Pep25 solution spread at the surface was 10 µL 0.33 mM Pep25 in pure water. Solutions were spread using a 25 µL Syringe (Hamilton Inc., Reno, Nevada) held less than 1 cm from the subphase surface. To standardize the function of the trough, a monolayer of 40 µL 1.55 mM stearic acid in dichloromethane was measured. All π-A isotherms were measured at a compression rate of 31.125 mm/minute.

2.7 Infrared Reflection Absorption Spectroscopy

Infrared Reflection Absorption Spectroscopy (IRRAS) was carried out on a EQUINOX 55 Fourier transform infrared spectrometer (Bruker Optics, Billerica, MA, USA) equipped with a XA-511 external reflection accessory with a mercury–cadmium–telluride detector cooled by liquid nitrogen. IRRAS was carried out on a film of 35 µl 1.0 mg/mL Pep25 on phosphate buffered saline pH 11.5 solution subphase compressed to a surface pressure of 10 mN/m on a Kibron µ-trough S (Kibron Inc., Helsinki, Finland) Langmuir Trough. IRRAS spectra were collected at incident angles of 36°, 41°, 47°, 52°, 58°, 63°, 69°, and 74° from the normal of the air-water interface. These angles were chosen to maximize absorbance. Each spectrum was collected using p-polarized light with a co-addition of 1200 scans with a resolution of 8 cm^{-1}.

2.8 Circular Dichroism Spectroscopy

Circular dichroism (CD) spectroscopy is used in conjunction with IRRAS to confirm that Pep25 remains in α-helix conformation at pH 12. CD is accomplished by measuring the degree and direction of polarization of light transmitted through the solution containing the molecule of interest. The CD spectrum between 180 and 260 nm, the carbonyl UV absorption region, can be measured to interpret the average secondary structure of a polypeptide [58]. Clear CD signals of α-helix, β-sheet and unstructured conformation have been catalogued.[58] CD spectroscopy was carried out on a Jasco model J-810 spectropolarimeter using a 150-W xenon lamp source. For the CD spectrum of Pep25, two scans were averaged, the scan speed was 20 nm/minute with a response time of 4 seconds. The analyte solution was 0.1 M pH 12.0 phosphate bufffered saline, 1mg/mL Pep25, the spectrum was taken through 1 mm path length quartz cells.

2.9 Materials Used

The materials used in this research and the respective suppliers are listed as follows. Tyrosine for UV-spectroscopy, and piperidine used for Fmoc deprotection were purchased from Sigma-Aldrich (St. Louis, MO). The materials used for peptide synthesis are listed as follows. Fmoc-Alanine, Fmoc-Lysine-OH, Fmoc-Tyrosine-OtBu, and Wang Resin were purchased from Novabiochem, (Hohenbrunn, Germany), Diisopropylcarbodiimide and hydroxybenzoyltriazole were purchased from Anaspec Inc. (Fremont, CA), and 4-dimethylaminopyridine was purchased from Acros Organics (New Jersey, USA). Dichloromethane, acetonitrile, diethyl ether, and dimethylformamide were purchased from Fisher Scientific (Fairlawn, NJ). Nitrogen gas was purchased from Airgas (Radnor, PA).

CHAPTER 3. RESULTS

3.1 HPLC Chromatograms of Pep25

A representative HPLC chromatogram of Pep25 is shown in Figure 15. Pep25 was collected from 6 HPLC runs (not shown) of samples containing 30-50 mg crude synthetic pep25 dissolved in 3-5 ml of 1:9 acetonitril/water (v/v). A. Pep25 has an average retention time of 19.82 minutes with a standard deviation of n minutes, as measured by UV absorbance at 220 and 275 nm. The collection window (i.e. the time the eluent was collected before and after the peak retention time) for each HPLC run was 0.5 minutes with a standard deviation of 0.1 minutes. The fraction with this retention time was confirmed to be Pep25 by mass spectrometry as shown in section 3.2. The other visible peaks represent impurities and synthetic by-products in the crude synthetic product Pep25, from which it was separated from. This peak was collected with as the purified fraction of the crude synthetic product and lyophilized to obtain pure Pep25, as confirmed by the mass spectrum in the following section.

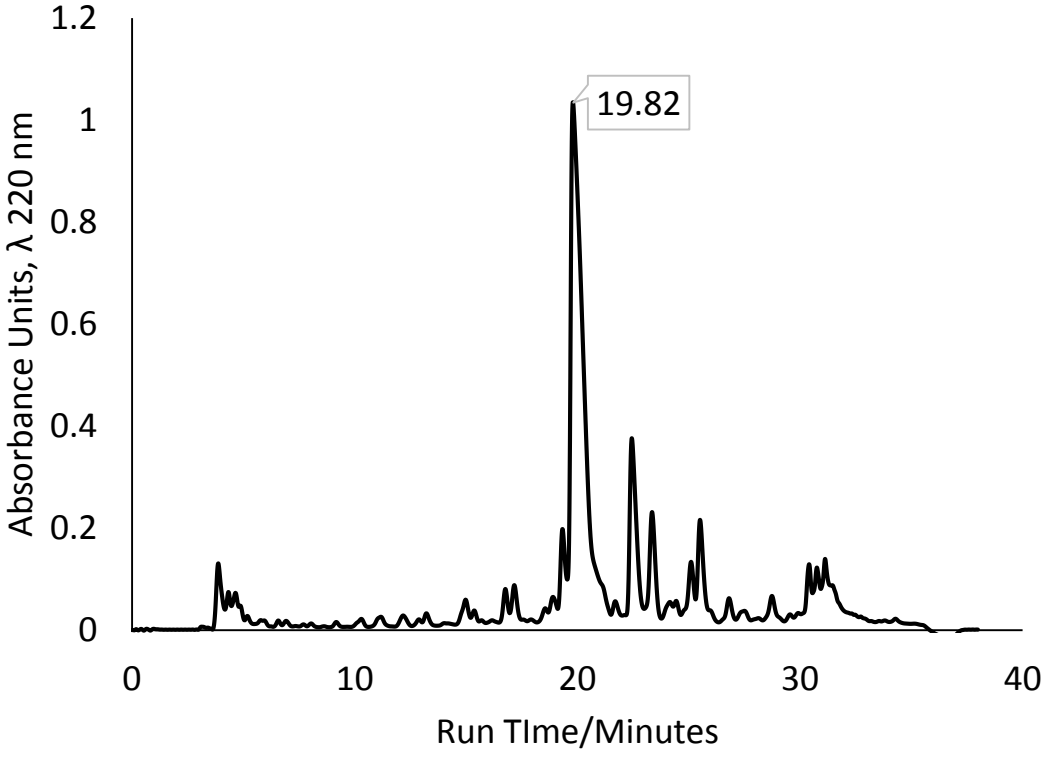

Figure 15. Representative HPLC chromatogram of Pep25.

3.2 Mass Spectra of Pep25

The HPLC purified Pep25 was analyzed by Mass spectrometry and the results are shown in Figure 16. The peak appearing at 1058.4 is assigned to the double protonated Pep25 with chemical formula $C_{93}H_{161}N_{29}O_{27}^{2+}$, which has a chemical formula of $C_{93}H_{159}N_{29}O_{27}$ from which the theoretical average MW is 2115.3. The $(M+3H)^{3+}$ ion of Pep25 with chemical formula $C_{93}H_{162}N_{29}O_{27}^{3+}$ appears at 706.3 and the $(M+4H)^{4+}$ ion of Pep25 with chemical formula $C_{93}H_{163}N_{29}O_{27}^{4+}$ appears at 529.7. A value of 2114.6 Da is calculated from the double protonated peak and assigned to Pep25, which is very close to the theoretical value of 2115.3 Da. To confirm the sequence of Pep25 precisely as shown in Figure 2 MS/MS fragmentation analysis was employed and the results are shown in the next section.

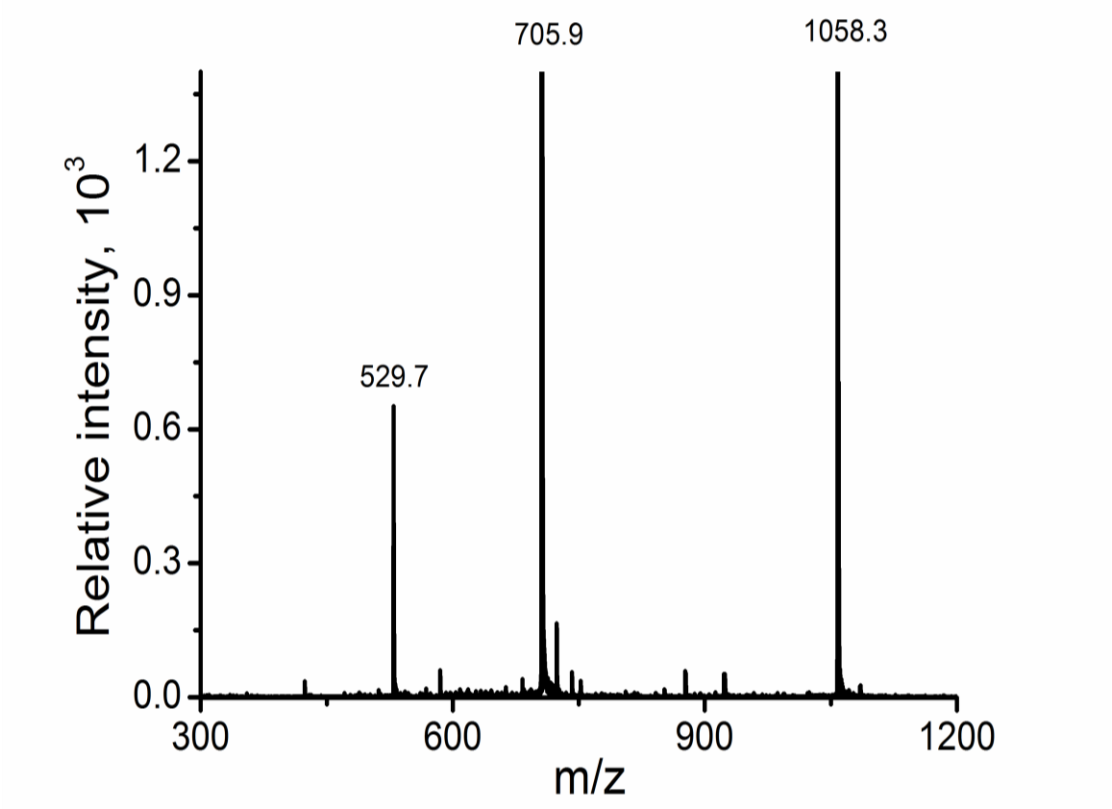

Figure 16. Mass spectrum of Pep25.

3.3 Confirmation of the Sequence of Pep25 by MS/MS

The fragment MS/MS spectrum of unlabeled Pep25 is shown in Figure 17. Notice that the standard deviation of the fragment MS measurement increases slightly when compared with the MS spectra measurement as shown in Figure 16. Thus, the molecular peak of unlabeled Pep25 detected at 2115.1 Da is reasonably close to the theoretical value as mentioned previously (c.f. section 3.2). All of the possible MS/MS fragment sequences are listed in Table 4, for this table, peptides are written from C- to N-terminus, the reverse of the direction of the primary structure in Figure 1. If the three C-terminal alanine (i.e., AAA) are removed by collision gas (Ion A), the sequence of

AAKAAAAKAAAAKAAAAKAAAAY (theoretical formula weight of 1884.2 Da shown in the line 3 of Table 4) is generated (Ion B) and detected at 1883.9 Da in Figure 17. At the same time, the fragment of AAA is also detected at 231.1. All of the N-terminal fragment sequences and their counterpart C-terminal sequences listed in Table 3.1 are detected and shown in Figure 17. Thus, the sequence of unlabeled Pep25 can be confirmed. Other peaks that are not listed in Table 4 are also detected in Figure 17, because the MS/MS fragments were also generated when other bonds (not amide bond) were broken. Because there were many types of small fragments generated, the peaks of M/Z values under 200 are not distinguishable. Consequently, the data of M/Z below 200 was not included in Figure 17 and Table 4.

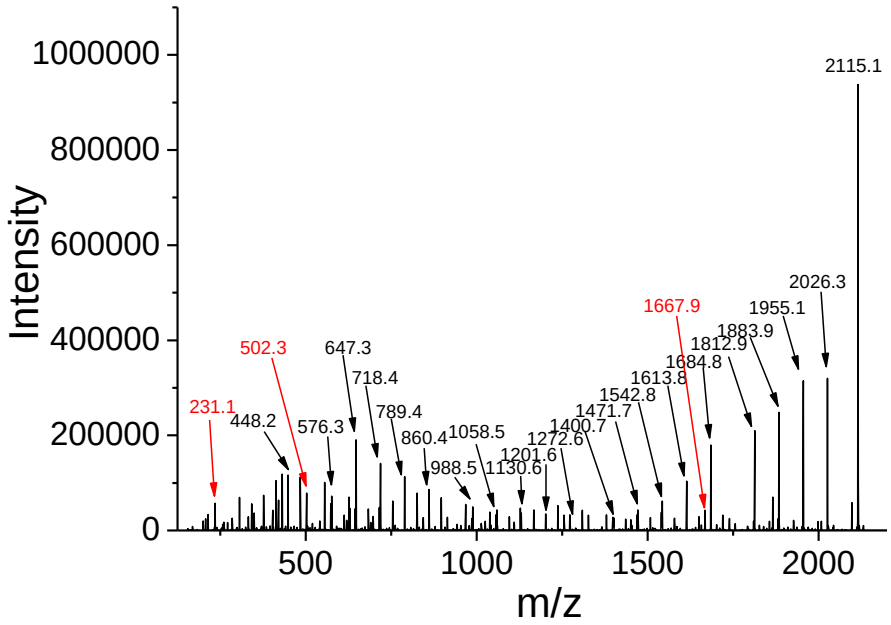

Figure 17. Fragment MS/MS Spectrum of Pep25. Fragments are singly charged with one proton. The fragment peaks of C-terminal (Ion A) sequences are labeled in red and

the peaks of N-terminal (Ion B) sequences are labeled in Black. Due to the limitation of space, only three N-terminal (Ion A) sequences are labeled.

Table 4. Fragments of Pep25 with the theoretical formula weight and the detected formula weight as the M/Z ratio.

Fragment of N-terminal sequence (Ion A)	Theoretical m/z	Detected m/z	Counterpart C-terminal sequence (Ion B)	Theoretical m/z	Detected m/z
AAAKAAAAKAAAAKAAAAKAAAAY	2026.4	2026.3	A	89.1	N/A
AAKAAAAKAAAAKAAAAKAAAAY	1955.3	1955.1	AA	160.2	N/A
AKAAAAKAAAAKAAAAKAAAAY	1884.2	1883.9	AAA	231.3	231.1
KAAAAKAAAAKAAAAKAAAAY	1813.1	1812.9	AAAA	302.4	303.1
AAAAKAAAAKAAAAKAAAAY	1685.0	1684.8	AAAAK	430.5	431.2
AAAKAAAAKAAAAKAAAAY	1613.9	1613.8	AAAAKA	501.6	502.3
AAKAAAAKAAAAKAAAAY	1542.8	1542.8	AAAAKAA	572.7	573.3
AKAAAAKAAAAKAAAAY	1471.7	1471.7	AAAAKAAA	643.8	644.3
KAAAAKAAAAKAAAAY	1400.7	1400.7	AAAAKAAAA	714.9	715.4
AAAAKAAAAKAAAAY	1272.5	1272.6	AAAAKAAAAK	843.0	843.5
AAAKAAAAKAAAAY	1201.4	1201.6	AAAAKAAAAKA	914.1	914.5
AAKAAAAKAAAAY	1130.3	1130.6	AAAAKAAAAKAA	985.2	985.6

AKAAAAKAAAAY	1059.2	1058.5	AAAAKAAAAKAAA	1056.3	1056.6
KAAAAKAAAAY	988.2	988.5	AAAAKAAAAKAAAA	1127.3	1127.6
AAAKAAAAY	860.0	860.4	AAAAKAAAAKAAAAKA	1255.5	1255.7
AAKAAAAY	788.9	789.4	AAAAKAAAAKAAAAKAA	1326.6	1326.8
AKAAAAY	717.8	718.4	AAAAKAAAAKAAAAKAAA	1397.7	1397.8
KAAAAY	646.8	647.3	AAAAKAAAAKAAAAKAAAA	1468.8	1468.8
AAAAY	575.7	576.3	AAAAKAAAAKAAAAKAAAAK	1539.8	1539.8
AAAY	447.6	448.2	AAAAKAAAAKAAAAKAAAAKA	1668.0	1667.9

3.4 Determination of the Concentration of Pep25 by UV-Vis Spectroscopy

After HPLC purification, there is still some solvent molecules and a hydration shell of water molecules remaining in the solid Pep25 sample. To determine the concentration of the Pep25 in aqueous solution accurately, Beer's law was used for quantitative calibration by plotting the aborbance of the tyrosine (Y) residue near 275 nm. The UV-Vis absorption of tyrosine amino acid was shown in Figure 18. The extinction coefficient was found to be 1206.8 ($M^{-1}cm^{-1}$) with a R^2 value of 0.999, the concentration of Pep25 is determined to be 0.33 mM for the surface pressure-area measurements.

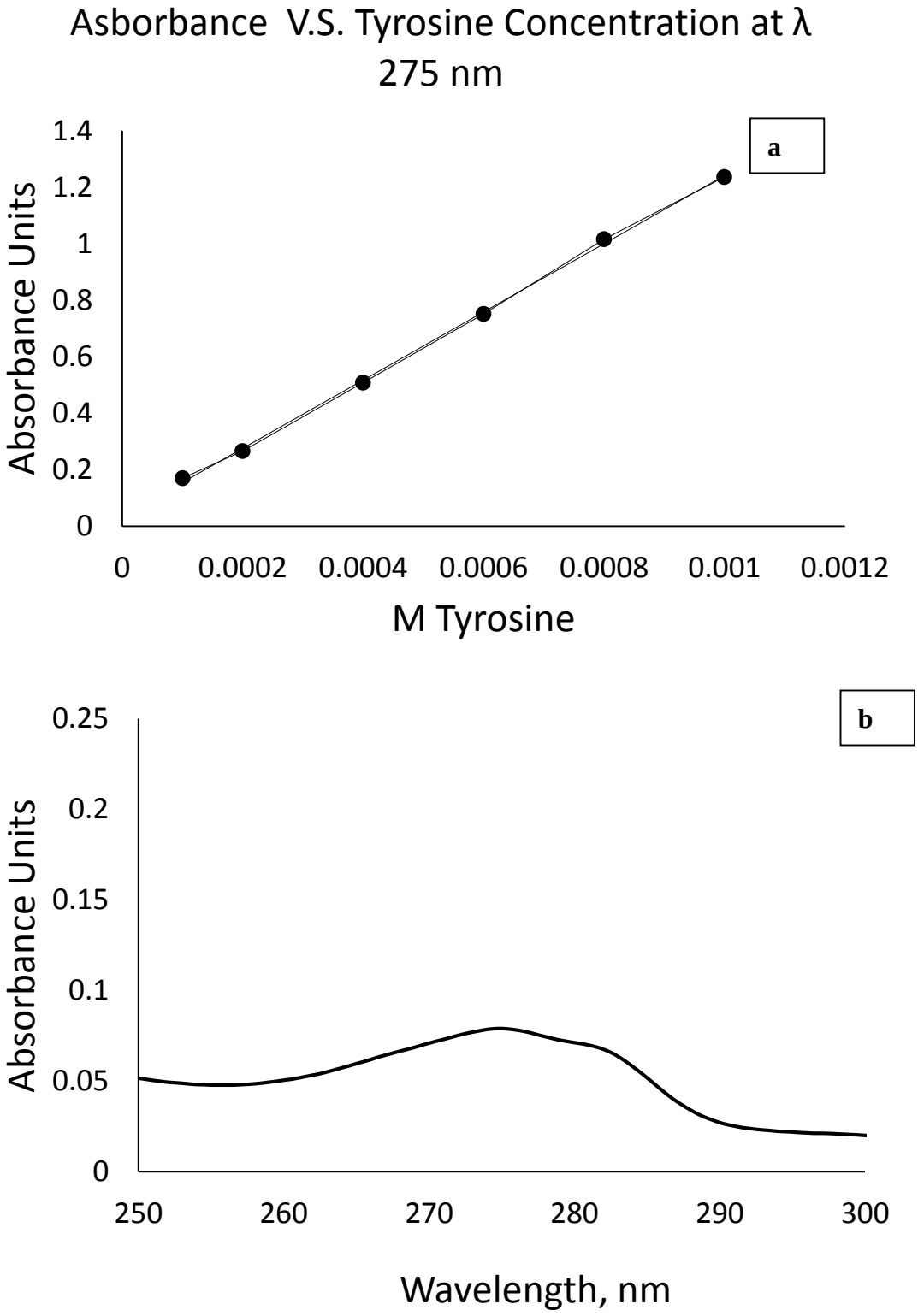

Figure 18. Calibration curve of Tyr (a, top), absorbance of Pep25 solution (b. bottom.).

3.5 π-A Isotherm of Stearic Acid

Prior to carrying out Langmuir trough measurements on Pep25, a π-A isotherm of stearic acid on pure water subphase was measured and compared to literature values in order to standardize the function of the Langmuir trough, the results are shown in Figure 19. The lift-off point of around 26 $Å^2$/molecule and surface pressure increased rapidly to a kink point at 21 $Å^2$/molecule. After the kink point, the surface pressure increased sharply until collapse. Both the shape and the molecular area of lift-off point as well as the kink point are identical to the results acquired by Hwang and coworkers.[37] This verified that the Langmuir monolayer trough functions accurately.

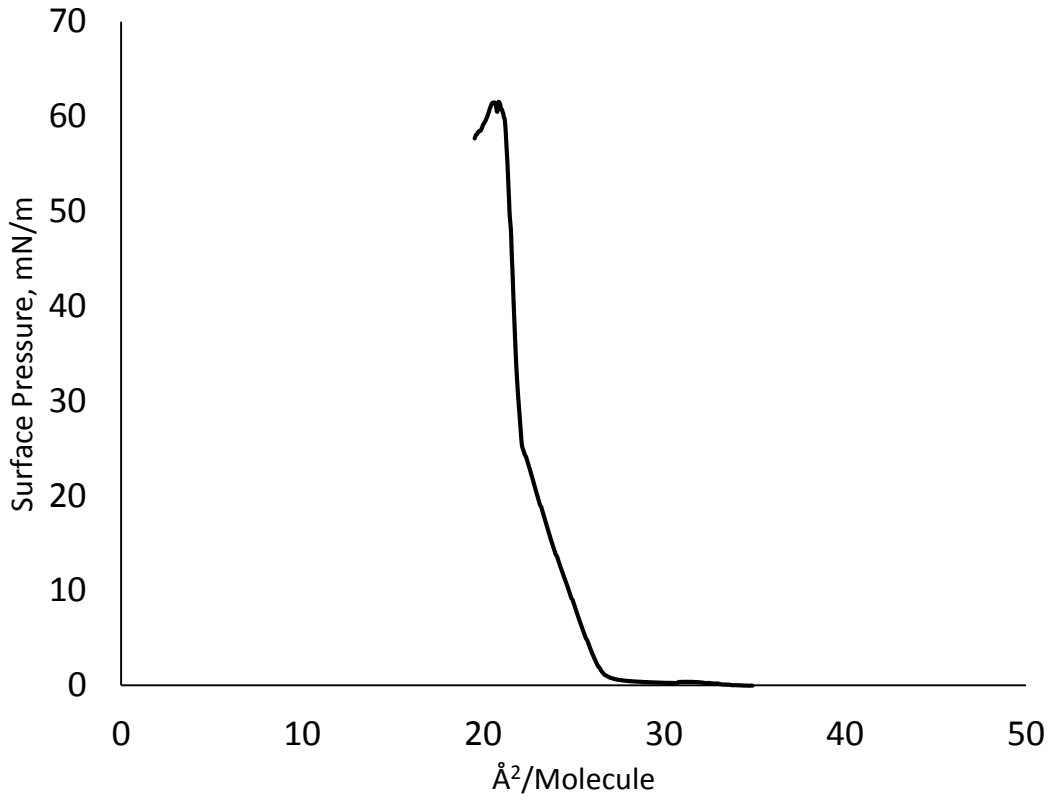

Figure 19. π -A isotherm of stearic acid.

3.6 π-A isotherms of Pep25 On Various pH Subphases

The π-A isotherms of Pep25 at various pH are shown in Figure 20. As for pure water subphase at pH 5.5, the lift-off point was around 200 $Å^2$/molecule and the surface pressure increase slowly until a kink point around 70 $Å^2$/molecule, which is small compared with that of α-synuclein at around 1500 $Å^2$/molecule. If Pep25, which has 25 residues, forms a typical Langmuir monolayer (LM), the kink point should be around 250 $Å^2$/molecule according to the fact that α-synuclein contains 140 residues. This indicates that Pep25 did not form a typical LM. The pH was increased in an attempt to deprotonate and neutralize the NH_3^+ in lysine, because the lysine in the sequence may contain hydrophilic residue group NH_3^+ with pKa value around 10.5, to make Pep25 less hydrophilic in an attempt to cause it to form typical LM. Increasing the pH to 7.0 increased the kink point to 120 $Å^2$/molecule. When the pH was further increased to 10.0 and 11.5, the molecular area of the kink point further increased. However, the surface pressure does not increase at a constant linear rate after the kink point. This indicates that a typical LM does not form with increasing pH values, which was confirmed by p-polarized IRRAS as shown below.

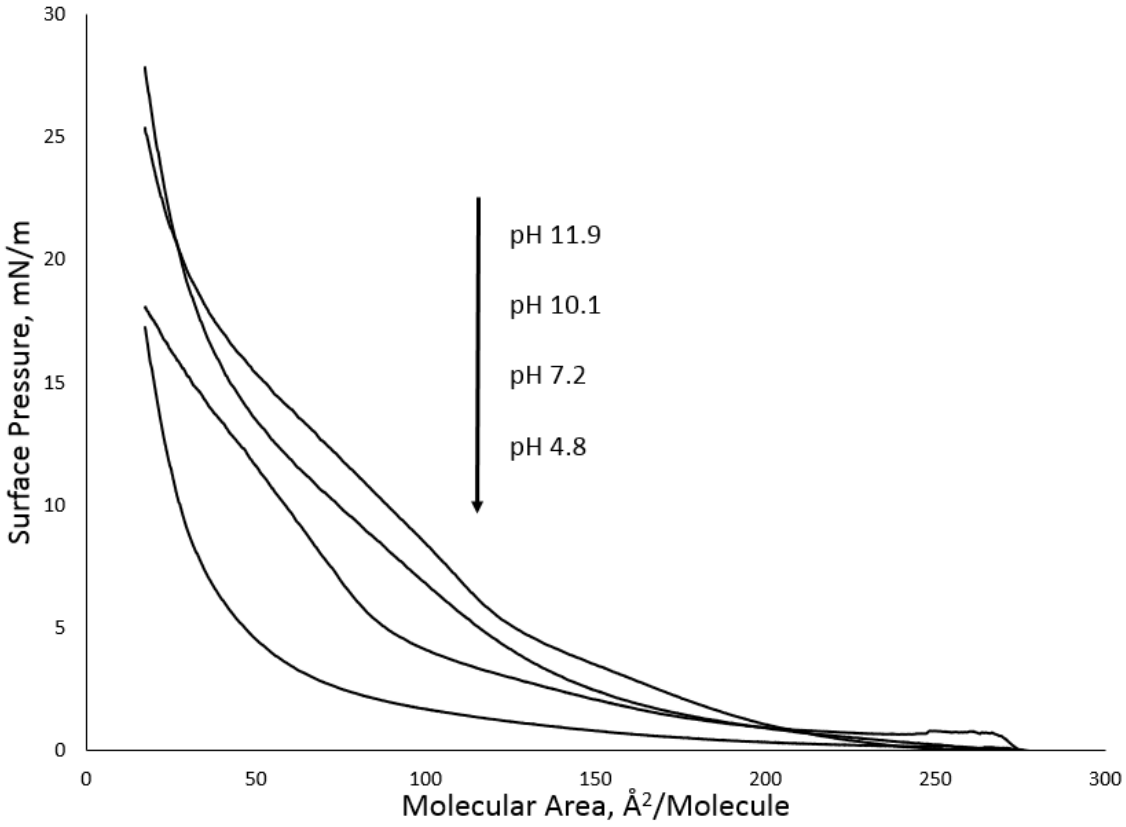

Figure 20. πA isotherms of Pep25 at different pH values.

3.7 P-Polarized IRRAS of Pep25 at the Air-Water Interface

The p-polarized IRRAS of the Pep25 at the air-water interface with pH 5.0 are shown in Figure 21 with incident angles from 36 º to 74º. The Amide I band was detected at 1650 cm^{-1}, which is a typical position of α-helix. The peak was negative at angles below the Brewster angle and became very weak with the increasing incident angle. We also measured the IRRAS of Pep25 at pH 5 which indicates α-helix conformation (results not shown). This indicates that Pep25 does not form a typical

monolayer at the air-water interface and more detailed discussion is presented in the following chapter.

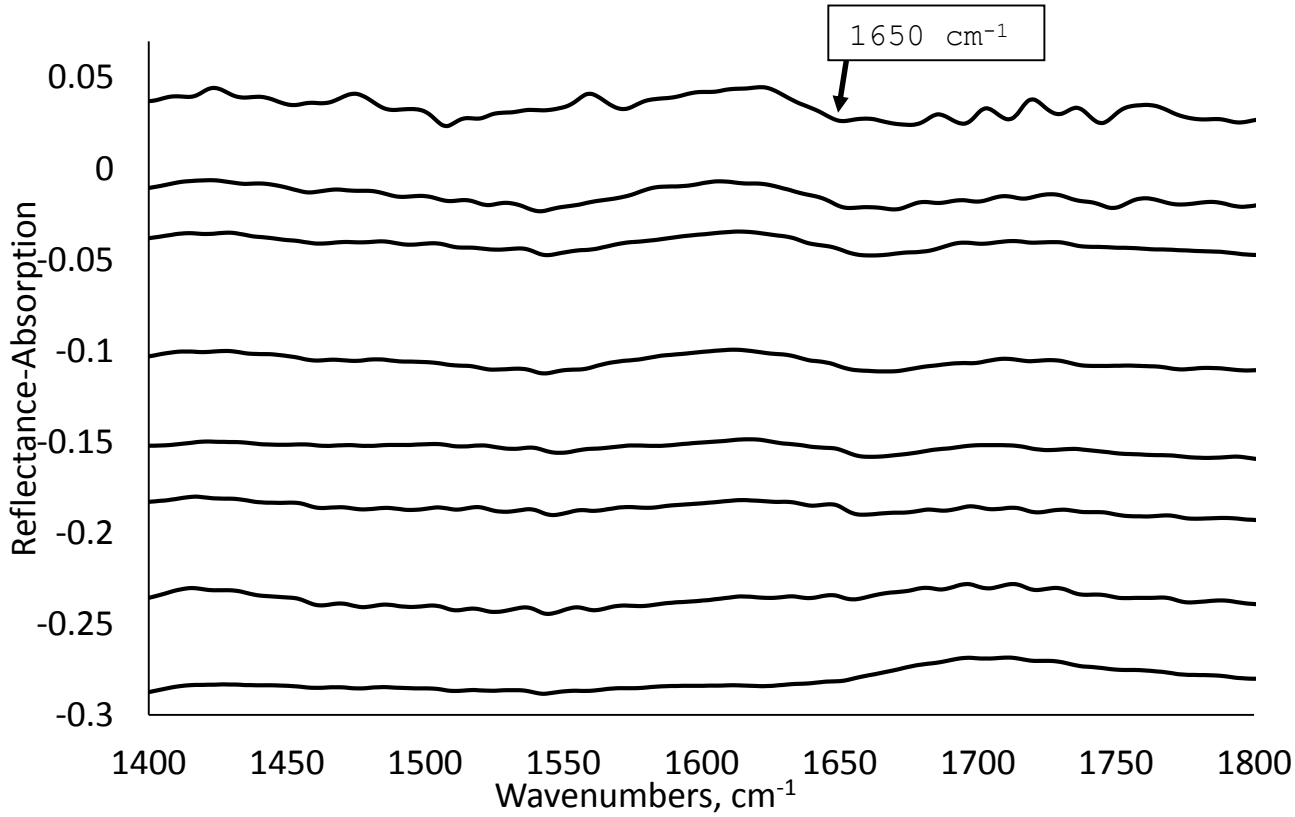

Figure 21. p-Polarized IRRAS of Pep25 at 10 mN/m surface pressure at increasing incident angles of (top → bottom) 36 °, 41 °, 47 °, 52 °, 58 °, 63 °, 69 °, and 74 °.

3.8 CD Spectroscopy of Pep25

To investigate potential conformation change induced by pH increase, CD spectra of Pep25 at pH 10.1 and 11.9 were measured. The characteristic two negative peaks of helix appeared in the CD spectra of Pep25 at pH 10.1 and 11.9. Thus, Pep25 was in α-helix under high pH values; there is no conformation change induced by these pH values. The results from CD spectroscopy are shown below in Figure 22. The CD

spectrum shows two negative peaks at 208 nm and 222 nm for both pH values which indicate an α-helical conformation.[57] This confirms that pep25 is in α-helix near pH 12.

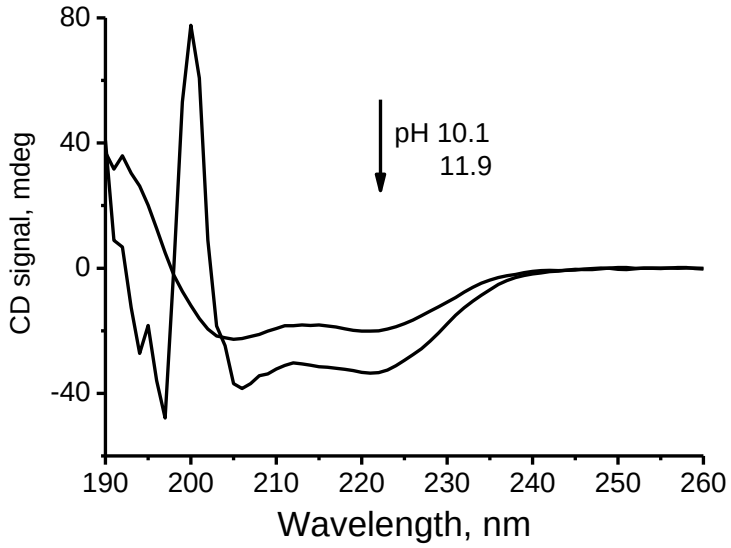

Figure 22. CD spectra of Pep25 at pH 10.1 and 11.9.

CHAPTER 4. DISCUSSION AND FUTURE PRESPECTIVES

4.1 Pep25 Does Not Form a Typical LM

As shown in Figure 3.5, the molecular area was with a pure water or pH 7.0 buffer subphase. As shown in **Chapter 1**, the molecular area of stearic acid which contains one alkyl chain is about 21 $Å^2$/molecule, which is close to the value of Pep25 on pure water subphase. Notice that the MW of Pep25 is much larger than that of stearic acid. In addition, the surface pressure increases slowly after the lift-off point of Pep25 at the air-water interface. Furthermore, a weak amide I band with peak intensity around 0.002 was detected in the IRRAS of Pep25 at the air-water interface. This value was much lower than a typical peak intensity about 0.005 of the Langmuir monolayer of protein.[2] All of the results support the conclusion that Pep25 remains at the air-water interface but does not form a typical Langmuir monolayer.

4.2 Impact of Lysine Residues on the Surface Properties of Pep25

The lift-off point increased with increasing pH, especially when the pH increased to values similar to the pKa of the residue group (i.e., $-NH_3^+$) of lysine at 10.5. As the CD results presented in Section 3.8 indicate no conformation change occurs upon elevating the pH, we attribute the increment of the molecular area of the kink point of Pep25 to the neutralization of the NH_3^+ in lysine. After deprotonation from $–NH_3^+$ to $–NH_2$, the residue group of lysine becomes more hydrophobic due to the reduction in charge. We attribute the stronger tendency of Pep25 to stabilize at the air-water interface and the increase the area of the lift-off point to its loss of charge.

4.3 Length of α-Helical Backbone Segments and Peptide Surface Phoperties

It has been clearly shown that an α-helical peptide with more than 100 residues can form a typical Langmuir monolayer.[2] We tried to determine a shorter length of α-helical peptide to form Langmuir monolayer in this thesis. However, Pep25 shows a tendency to go to the interface but does not form a typical Langmuir monolayer. We also tried to study the surface properties of another model α-helical peptide with a sequence of HAAKAAAAKAAAAKAAY, which showed similar surface properties of Pep25 (results not shown). We did try to study an even shorter peptide with sequence AAAAKAAAAK but this ten residue peptide does not form α-helical conformation (results not shown). In general, we have studied the short peptides with α-helical conformation and detect the tendency of the peptides to have a comparatively high concentration at the interface relative to the solution.

4.4 Future Perspectives

To study the length of an α-helical peptide able to form a stable and typical Langmuir monolayer, a longer peptide will be synthesized. On the other hand, phospholipids molecules may help to stabilize Pep25 at the air-water interface. As discussed in Chapter 1, phospholipids contain two alkyl chains and a hydrophilic head group. It has been shown that phospholipids can form stable and typical Langmuir monolayer.[59] Due to the positive charges in the residue group of Pep25, the Langmuir monolayer of phospholipids with negative charges (such as

dipalmitoylphosphatidylserine) may have strong electrostatic interaction with Pep25 and stabilize Pep25 at the air-water interface.

REFERENCES

1. Cherepanov, D. A.; Feniouk, B. A.; Junge, W.; Mulkidjanian, A. Y. Low dielectric permittivity of water at the membrane interface: Effect on the energy coupling mechanism in biological membranes *Biophys. J.* **2003**, *85*, 1307.

2. Wang, C.; Shah, N.; Thakur, G.; Zhou, F.; Leblanc, R. M. a-Synuclein in a-helical conformation at the air-water interface: Implication of conformation and orientation changes during its accumulation/aggregation *Chem. Commun.* **2010**, *46*, 6702.

3. Kobko, N.; Paraskevas, L.; del Rio, E.; Dannenberg, J. Cooperativity in amide hydrogen bonding chains: Implications for protein-folding models *J. Am. Chem. Soc.* **2001**, *123*, 4348.

4. Lam, R. S. H.; Nickerson, M. T. Food proteins: A review on their emulsifying properties using a structure-function approach *Food Chem.* **2013**, *141*, 975.

5. Peters, D.; Peters, J. Structure and bonding in proteins: Electron organization in amide unit *J. Mol. Struct.* **1978**, *50*, 133.

6. Sachs, J. N.; Engelman, D. M. Introduction to the membrane protein reviews: The interplay of structure, dynamics, and environment in membrane protein function *Ann. Rev. Biochem.* **2006**, *75*, 707.

7. Greenwald, R. A. Superoxide-dismutase and catalase as therapeutic agents for human diseases, a critical review *Free Radical Biol. Med.* **1990**, *8*, 201.

8. Loredo-Trevino, A.; Gutierrez-Sanchez, G.; Rodriguez-Herrera, R.; Aguilar, C. N. Microbial enzymes involved in polyurethane biodegradation: A review *J. Polymers Envir.* **2012**, *20*, 258.

9. Srikanth, K.; Pereira, E.; Duarte, A. C.; Ahmad, I. Glutathione and its dependent enzymes' modulatory responses to toxic metals and metalloids in fish-a review *Environ. Sci. Pollut. Res.* **2013**, *20*, 2133.

10. Testa, B.; Pedretti, A.; Vistoli, G. Foundation review: Reactions and enzymes in the Metabolism of drugs and other Xenobiotics *Drug Disc. Today* **2012**, *17*, 549.

11. Wevers, R. A.; de Rijk-van Andel, J. F.; Brautigam, C.; Geurtz, B.; van den Heuvel, L.; Steenbergen-Spanjers, G. C. H.; Smeitink, J. A. M.; Hoffmann, G. F.; Gabreels, F. J. M. A review of biochemical and molecular genetic aspects of tyrosine hydroxylase deficiency including a novel mutation (291delC) *J. Inherited Metabolic Dis.* **1999**, 364.

12. McCauley, M. J.; Williams, M. C. Review: Optical tweezers experiments resolve distinct modes of DNA-protein binding *Biopolymers* **2009**, *91*, 265.

13. Dubnau, D. Binding and transport of transforming DNA by Bacillus subtilis: The role of type-IV pilin-like proteins - A review *Gene* **1997**, *192*, 191.

14. Appert-Collin, A.; Baisamy, L.; Diviani, D. Review - Regulation of G protein-coupled receptor signaling by A-kinase anchoring proteins *J. Receptors Sign. Trans.* **2006**, *26*, 631.

15. Mizejewski, G. J. Review of the putative cell-surface receptors for alpha-fetoprotein: identification of a candidate receptor protein family *Tumor Biol.* **2011**, *32*, 241.

16. Chautard, E.; Thierry-Mieg, N.; Ricard-Blum, S. Interaction networks: From protein functions to drug discovery. A review *Path. Biol.* **2009**, *57*, 324.

17. Smythies, J.; Galzigna, L. The oxidative metabolism of catecholamines in the brain: a review *Biochim. Biophys. Acta.* **1998**, *1380*, 159.

18. Varadarajan, S.; Yatin, S.; Aksenova, M.; Butterfield, D. A. Review: Alzheimer's amyloid b-peptide-associated free radical oxidative stress and neurotoxicity *J. Struct. Biol.* **2000**, *130*, 184.

19. Wright, J. A.; Brown, D. R. Alpha-synuclein and its role in metal binding: Relevance to Parkinson's disease *J. Neurosci. Res.* **2008**, *86*, 496.

20. Deisenhofer, J.; Epp, O.; Miki, K.; Huber, R.; Michel, H. Structure of the protein subunits in the photosynthetic reaction centre of Rhodopseudomonas viridis at 3Å resolution *Nature* **1985**, *318*, 918.

21. Petry, S.; Brodersen, D. E.; Murphy, F. V.; Dunham, C. M.; Selmer, M.; Tarry, M. J.; Kelley, A. C.; Ramakrishnan, V. Crystal structures of the ribosome in complex with release factors RF1 and RF2 bound to a cognate stop codon *Cell* **2005**, *123*, 1255.

22. Pfister, P.; Corti, N.; Hobbie, S.; Bruell, C.; Zarivach, R.; Yonath, A.; Bottger, E. C. 23S rRNA base pair 2057-2611 determines ketolide susceptibility and fitness cost of the macrolide resistance mutation 2058A -> G *Proc. Natl. Acad. Sci. U. S. A.* **2005**, *102*, 5180.

23. Steitz, T. A. A structural understanding of the dynamic ribosome machine *Nat. Rev. Mol. Cell Biol.* **2008**, *9*, 242.

24. Adessi, C.; Soto, C. Beta-sheet breaker strategy for the treatment of Alzheimer's disease *Drug Development Res.* **2002**, *56*, 184.

25. Pauling, L.; Corey, R. B. Configurations of polypeptide chains with favored orientations around single bonds *Proc. Nat. Acad. Sci. U.S.A.* **1951**, *37*, 729.

26. Floudas, C. A.; Fung, H. K.; McAllister, S. R.; Monnigmann, M.; Rajgaria, R. Advances in protein structure prediction and de novo protein design: A review *Chem. Engin. Sci.* **2006**, *61*, 966.

27. Robinson, N. E.; Robinson, A. B. Review article: Use of Merrifield solid phase peptide synthesis in investigations of biological deamidation of peptides and proteins *Biopolymers* **2008**, *90*, 297.

28. Zhu, M.; Fink, A. L. Lipid binding inhibits a-synuclein fibril formation *J. Biol. Chem.* **2003**, *278*, 16873.

29. Teschke, O.; de Souza, E. F. Liposome structure imaging by atomic force microscopy: Verification of improved liposome stability during adsorption of multiple aggregated vesicles *Langmuir* **2002**, *18*, 6513.

30. Won Jin Cho, A. J., Huan Jin, Hang Ren, Bhanu P. Jena Neuronal fusion pore assembly requires membrane cholesterol *Cell Biology International* **2007**, *31*, 1301.

31. Ewa Paluch, C.-P. H. Biology and Physics of Cell Shape Changes in Development *Current Biology* **2009**, *19*, 790.

32. R. O. Blaustein, A. F. Voltage-dependent block of anthrax toxin channels in planar phospholipid bilayer membranes by symmetric tetraalkylammonium ions. Effects on macroscopic conductance *J. Gen. Physiol.* **1990**, *96*, 905.

33. H. Lodish, A. B., S. L. Zipursky In *Molecular Cell Biology.*; 4 ed.; W. H. Freeman: New York, 2000.

34. S. Oiki, V. M., M. Montal Bundles of amphipathic transmembrane alpha-helices as a structural motif for ion-conducting channel proteins: studies on sodium channels and acetylcholine receptors *Proteins* **1990**, *8*, 226.

35. Alireza Mashaghi, P. P.-A., Tayebeh Jadidi, Nasser Nafari, Philipp Maass, M. Reza Rahimi Tabar, Mischa Bonn,Huib J. Bakker Hydration strongly affects the molecular and electronic structure of membrane phospholipids *The Journal of Chemical Physics* **2012**, *136*.

36. Michael J. Higgins, M. P., Takeshi Fukuma, John E. Sader, Yshikazu Nakayama Structured Water Layers Adjacent to Biological Membranes *Biophysical Journal* **2006**, *91*, 2532.

37. Mi-Ja Hwang, K. K. Poly(ethylenimine) as a Subphase Stabilizer of Stearic Acid Monolayers at the Air/Water Interface: Surface Pressure-Area Isotherm and Infrared Spectroscopy Study *Langmuir* **1999**, *15*, 3563.

38. Wang, C.; Liu, L.; Zhang, L.; Peng, Y.; Zhou, F. Redox reactions of the a-synuclein-Cu^{2+} complex and their effects on neuronal cell viability *Biochemistry* **2010**, *49*, 8134.

39. Wang, C.; Zheng, J.; Oliveira, O. N.; Leblanc, R. M. Nature of the interaction between a peptidolipid Langmuir monolayer and paraoxon in the subphase *J. Phys. Chem. C* **2007**, *111*, 7826.

40. Hasegawa, T.; Nishijo, J.; Watanabe, M.; Umemura, J.; Ma, Y.; Sui, G.; Huo, Q.; Leblanc, R. M. Characteristics of long-chain fatty acid monolayers studied by infrared external-reflection spectroscopy *Langmuir* **2002**, 4758.

41. Thakur, G.; Leblanc, R. M. Conformation of lysozyme Langmuir monolayer studied by Infrared Reflection Absorption Spectroscopy *Langmuir* **2009**, *25*, 2842.

42. Thakur, G.; Micic, M.; Leblanc, R. M. Surface chemistry of Alzheimer's disease: A Langmuir monolayer approach *Colloid. Surf. B* **2009**, *74*, 436.

43. Wang, C.; Micic, M.; Ensor, M.; Daunert, S.; Leblanc, R. M. Infrared reflection-absorption spectroscopy and polarization-modulated infrared reflection-absorption spectroscopy studies of the aequorin Langmuir monolayer *J. Phys. Chem. B* **2008**, *112*, 4146.

44. Jiang, D.; Men, L.; Wang, J.; Zhang, Y.; Chickenyen, S.; Wang, Y.; Zhou, F. Redox reactions of copper complexes formed with different b-amyloid peptides and their neuropathalogical relevance *Biochemistry* **2007**, *46*, 9270.

45. Wang, C.; Zheng, J.; Zhao, L.; Rastogi, V. K.; Shah, S. S.; DeFrank, J. J.; Leblanc, R. M. Infrared reflection-absorption spectroscopy and polarization-modulated Infrared Reflection-Absorption Spectroscopy studies of the organophosphorus acid anhydrolase Langmuir monolayer *J. Phys. Chem. B* **2008**, *112*, 5250.

46. Du, X.; Miao, W.; Liang, Y. IRRAS studies on chain orientation in the monolayers of amino acid amphiphiles at the air-water interface depending on metal complex and hydrogen bond formation with the headgroups *J. Phys. Chem. B* **2005**, *109*, 7428.

47. Jiang, D.; Dinh, K. L.; Tuthenburg, T. C.; Zhang, Y.; Su, L.; Land, D. P.; Zhou, F. A kinetic model for b-amyloid adsorption at the air/solution interface and its implication to the b-amyloid aggregation process *J. Phys. Chem. B* **2009**, *113*, 3160.

48. Dziri, L.; Desbat, B.; Leblanc, R. M. Polarization-modulated FT-IR spectroscopy studies of acetylcholinesterase secondary structure at the air-water interface *J. Am. Chem. Soc.* **1999**, *121*, 9618.

49. Hasegawa, T.; Moriya, D.; Kakuda, H.; Li, C.; Orbulescu, J.; Leblanc, R. M. Fibril-like aggregate formation of peptide carboxylate Langmuir films analyzed by surface pressure, surface dipole moment, and infrared spectroscopy *J. Phys. Chem. B* **2005**, *109*, 12856.

50. Dziri, L.; Desbat, B.; Leblanc, R. M. Polarization modulated FT-IR spectroscopy studies of acetylcholinesterase secondary structure at the air-water interface *J. Am. Chem. Soc.* **1999**, *121*, 9618.

51. Smith, B. M.; Oswald, L.; Franzen, S. Single-pass attenuated total reflection Fourier Transform Infrared Spectroscopy for the prediction of protein secondary structure *Anal. Chem.* **2002**, *74*, 3386.

52. Belbachir, K.; Lecomte, S.; Ta, H. P.; Petibois, C.; Desbat, B. Orientation of molecular groups of fibers in nonoriented samples determined by polarized ATR-FTIR spectroscopy *Anal. Bioanal. Chem.* **2011**, *401*, 3263.

53. Decatur, S. M. IR spectroscopy of isotope-labeled helical peptides: Probing the effect of N-acetylation on helix stability *Biopolymers* **2000**, *54*, 180.

54. Johannes Oehlke, E. K., Burkhard Wienser, Michael Beyermann, Michael Bienert Nonendocytic, amphipathicity dependent cellular uptake of helical model peptides *Protein and Peptide Letters* **1996**, *3*, 393.

55. Emelia Eiriksdottir, K. K., Ulo Langel, Gilles Divita, Sebastien Deshayes Secondary structure of cell-penetrating peptides controls membrane interaction and insertion *Biochimica et Biophysica Acta* **2010**, *1798*, 1119.

56. Wang, C.; Li, S.; Sneha, P.; Leblanc, R. M. Determination of model peptide in a-helix by ^{13}C isotope edited FTIR in regular water by ATR technique *Chem. Commun.* **2014**, *50*, 3931.

57. Shanghao Li, J. D. C., Olaa Eid Alharbi, Jing Kong, Chengshan Wang, Roger M. Leblanc The 13C amide I band is still sensitive to conformation change when the regular amide I band cannot be distinguished at the typical position in H2O *ChemComm* **2015**, *51*, 12537.

58. Sreerama, N.; Woody, R. W. Estimation of protein secondary structure from CD spectra: Comparison of CONTIN, SELCON and CDSSTR methods with an expanded reference set *Anal. Biochem.* **2000**, *282*, 252.

59. Maltseva, E.; Kerth, A.; Blume, A.; Mohwald, H.; Brezesinski, G. Adsorption of amyloid b(1-40) peptide at phospholipid monolayers *Chembiochem* **2005**, *6*, 1817.